Thirteenth Quarterly Progress Report

September 26 through December 26, 1988

NIH Contract N01-NS-5-2396

Speech Processors for Auditory Prostheses

Prepared by

Charles C. Finley, Blake S. Wilson and Dewey T. Lawson

Neuroscience Program Office
Research Triangle Institute
Research Triangle Park, NC 27709

This QPR is being sent to you before it has been reviewed by the staff of the Neural Prosthesis Program

CONTENTS

I. Introduction

The purpose of this project is to design and evaluate speech processors for auditory prostheses. Ideally, the processors will extract (or preserve) from speech those parameters that are essential for intelligibility and then appropriately encode these parameters for electrical stimulation of the auditory nerve. Work in the present quarter included the following:

1. Evaluation of several processing strategies, including the hybrid strategy proposed in the last progress report for this project, in follow-up studies with two patients (MC1 and MC2) implanted with the UCSF/Storz cochlear prosthesis;

2. Development of software for (a) automated archiving of results from tests of consonant and vowel identification and (b) constructing aggregate confusion matrices from various subsets of the archived data, specified in terms of five testing variables;

3. Development of software for Information Transmission (IT) analysis and Sequential Information Analysis (SINFA) of the aggregate confusion matrices indicated in point 2 above;

4. Continued preparation for studies with patients implanted with the Nucleus cochlear prosthesis, including (a) evaluation of alternative systems for external control of the subcutaneous receiver for that prosthesis, (b) initial development of TMS320C25 software for real-time emulation of processing strategies to be tested in studies with Nucleus patients, and (c) scheduling of patients;

5. Continued upgrade of the Cochlear Implant Laboratory at Duke, along the lines indicated in the last two progress reports for this project;

6. Presentation of project results at the 25th Anniversary Symposium of the Kresge Hearing Research Institute (Oct. 3-5) and at the Nineteenth Neural Prosthesis Workshop (Oct. 26-28);

7. Continued collaboration with the UCSF team on the development of the speech processor and transcutaneous transmission system for a next-generation cochlear prosthesis;

8. Completion of two manuscripts for the book Models of the Electrically Stimulated Cochlea (edited by J.M. Miller and F.A. Spelman); and

9. Continued preparation of other manuscripts, including one on our evaluation of two-channel "Breeuwer/Plomp" processors for cochlear implants (see QPR 8, this project) and one on ensemble models of neural discharge patterns evoked by intracochlear electrical stimulation (see QPR 8, NIH project N01-NS-3-2356).

The main part of the present report, on "Models of Neural Responsiveness to Electrical Stimulation," is a slightly modified version of one of the papers indicated in point 8 above. Details on points 1-5 and 7 will be presented in future reports.

II. Models of Neural Responsiveness to Electrical Stimulation

A. Introduction

In principle electrical stimulation of the cochlea is a simple process. Intracochlear electrodes, when stimulated, create electrical field patterns within the cochlea. In the vicinity of the neural elements, these fields appear as extracellular voltage gradients or profiles that are continuous along the entire length of the neurons. These extracellular voltage fields produce current flow into and out of the neural elements depending upon the local impedances of the neural membranes. If the neural elements are sufficiently depolarized, action potentials are generated that propagate along each cell's axon to the cochlear nucleus. Globally these events occur simultaneously but in varying degree across a population of nerve cells, producing a group or ensemble of neural responses to the stimulation.

In practice however the details of the stimulation process are governed by a number of complex physical, anatomical and physiological factors. These include the configuration and placement of electrodes, the type, shape and magnitude of the stimulus waveform, the impedance of the cochlear tissue, the location and fine detailed anatomy of surviving neural elements and the deterministic and stochastic characteristics of stimulated neural membranes. There is evidence that each of these factors plays a significant role in determining both the specific response properties of neural elements individually and the global characteristics of the neural ensemble response in general. At present the specific details of these mechanisms are not well understood.

This report describes an integrated field-neuron model that combines all aspects of the interface problem into a single structure. The model predicts, assuming a given electrode configuration, the extracellular electric field patterns in the vicinity of the target neural elements and then computes the resultant response from the fibers. The integrated field-neuron model is composed of two complementary models that treat each step of the stimulation process separately. The first model describes the extracellular fields for scala tympani electrode configurations of arbitrary geometry and scalar placement using three-dimensional finite-element modeling techniques. The extracellular field estimates are then fed to a lumped-element, electrical-

analog, neural response model that describes the response of a single fiber to external electrical stimulation. Two neural models are discussed. One is an estimator of the initial site of stimulation based on the second spatial derivative of the extracellular fields. This model assumes a uniform myelinated fiber lying in the electrical field. The other is a lumped-element, electrical-analog model that addresses specific anatomical and physiological features of the neurons that significantly affect the elements' responsiveness to external electrical fields.

The objective of the integrated field-neuron modeling approach is to better define the events and controlling factors involved in the interface between the electrode and neural elements and to create testable hypotheses that may be further evaluated in human and animal experimentation. In the following sections, the field and neural models are discussed separately. First, finite-element field calculations for several experimentally and clinically applied bipolar electrode systems are presented. Then initial stimulation sites for myelinated neurons are estimated using second spatial derivatives for each computed electric field condition. Next an expanded, anatomically and physiologically-based neural model is used to show the significance of the ganglion cell body in electrical stimulation. Finally, the limitations of these models are discussed and future model refinements are outlined.

B. Three-Dimensional Finite Element Field Model

A variety of electric field models have been proposed for the electrically-stimulated cochlea. These models include lumped-element transmission-line models [1, 2, 3, 13, 16, 24, 34, 38], closed-form analytical models [32, 35] and numerical finite-difference models [9, 43]. To further our understanding of the electrical-to-neural interface problem involved in the electrically stimulated cochlea, a field model must describe the electrical stimulus in the immediate vicinity of the target neural fibers. Most models have focused primarily on describing potential patterns within scala tympani. Existing field models are limited in their abilities to account for fine details of cochlear anatomy and electrode structure. The analytical approach must assume simplifying geometries to obtain closed form solutions, and the finite-difference method is limited in spatial resolution

for reasonable model size. This report describes the use of a three-dimensional, finite-element model of intracochlear electrical fields that alleviates these limitations. A two-dimensional version of this model has been published previously [7].

The present model assumes that impedances within the cochlea are purely resistive. This assumption is based on the experimental finding that measured scala tympani field potentials are frequency independent for frequencies below 12.5 kHz [36]. This assumption allows the field calculation to be treated as a static field problem. Simple scaling of electrode input potentials produces appropriately scaled field estimates. Time varying stimuli also may be evaluated readily without consideration of capacitive, charge-storage effects of tissue. The assumption of a purely resistive system for the present model should be considered as a first approximation only. The cited experimental work on field frequency dependence applies only to fields within scala tympani. Still open is the question of frequency dependence of fields in other parts of the cochlea, in particular in the habenula and along tracts containing myelinated axonal processes. Similarly, significant capacitive effects may appear in the case of cross-turn stimulation due to the myelinated neural fibers filling the core of the modiolus. Consideration of capacitive effects is left to later refinements of the model.

In its simplest form the finite element approach is a piece-wise approximation method in which the field region to be modeled is divided into small discrete elements. Here solid elements are used with each element being defined by the interconnection of six or eight vertices or nodes. Any one node may define the corner of any number of elements. Potentials within each element are described by planar functions based on the potentials at the element's nodes. Boundary potentials for each side of an element are interpolations of the potentials at the nodes which define each side. Regional resistivities are defined for each element, and node potentials are either fixed to preset values or allowed to vary freely. Iterative minimization of the energy in each element of the model system produces a field description based on the final potentials at the nodes. The general finite element method as applied to biological problems has been reviewed recently [23]. Coburn applied the technique to study two-dimensional field patterns during electrical stimulation of the spinal cord [4].

Figure 1 shows a two-dimensional, finite-element description of the cross section of a human cochlea. A bipolar electrode pair is mounted in a

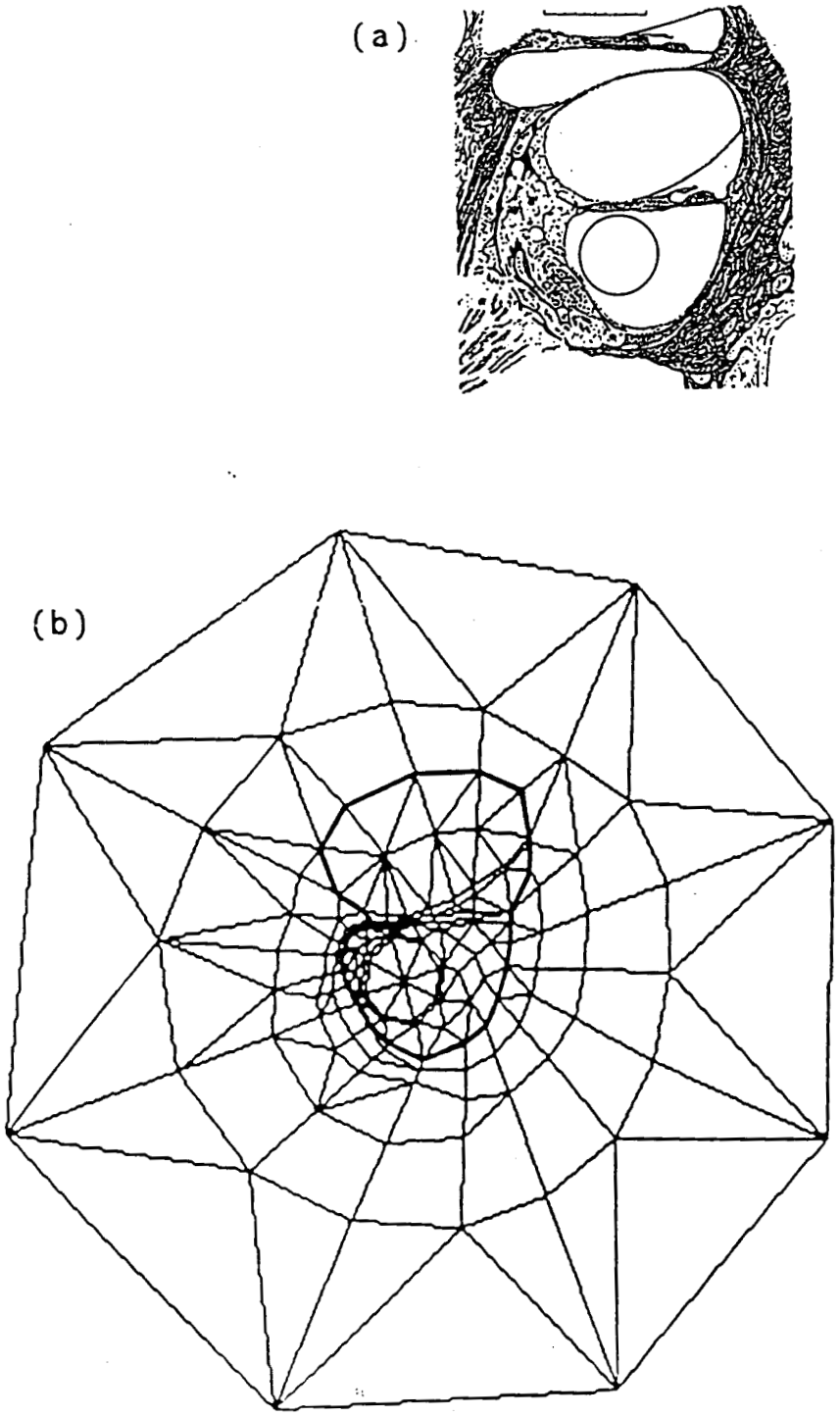

Figure 1. Two-dimensional, finite-element description of a cross section of a human cochlea. Panel (a) (reproduced with permission) shows a drawing of the histological section from [26] that is modeled in panel (b). A bipolar electrode pair mounted in a support insulator is included in the finite-element model representation. Note the higher spatial resolution in the central region of the cross section.

support insulator within scala tympani. Figure 1a is a drawing of a human histological cross section from [26]. A finite element representation of this section is shown in Figure 1b. This two-dimensional plane contains 152 nodes and 204 triangular and quadrilateral element profiles. Note that elements are smaller and more numerous in the central region of the plane thus increasing the spatial resolution of the model in that area. This plane is then expanded into a three-dimensional layer shown in Figure 2 by replicating the original node positions in a plane parallel to the original. A layer or slab consisting of five- and six-sided prisms is produced by defining three-dimensional elements that bridge these planes of nodes. Figure 3 shows an enlarged view of the scala region of the layer of Figure 2 with each element located in its original position in the layer but shrunk 15% geometrically. Here discrete anatomical regions that are modeled with different electrical resistivities are observable.

The model is further expanded by adding multiple parallel layers of varying thicknesses. Twelve layers constitute the final model as shown in Figure 4. This three-dimensional model represents a short straight section of the cochlear cross section projected linearly along an axis perpendicular to the plane of the section. No curvature of the cochlear spiral is modeled. Layer thicknesses, described in Figure 5, are graded to provide maximal spatial resolution in the center of the model.

Resistivities are defined regionally to characterize the electrodes, the carrier insulator, the endolymph, the perilymph, Reisner's membrane, basilar membrane, the anisotropic neural tissue leading down from the habenula to the spiral ganglion, the spiral ganglion itself, and bone. Table 1 describes the resistivities used in the model calculations presented in this report. All regions are assumed to be isotropic with the exception of the tract of the peripheral axonal processes between the habenula and ganglion. Electrode surfaces are modeled as simple metallic surfaces of low impedance. Complex access impedances, typical of real electrodes, are not considered in the present model. Such impedance characterization of the electrodes requires scaling of the electrode impedance on a regional basis depending upon electrode current density. The present model best describes systems in which the access impedance is low with respect to the impedance of the cochlear tissue itself. Regions outside of the model are treated as insulators, thus allowing node potentials along the outer periphery to vary.

The modeling of specific electrode geometries requires slight

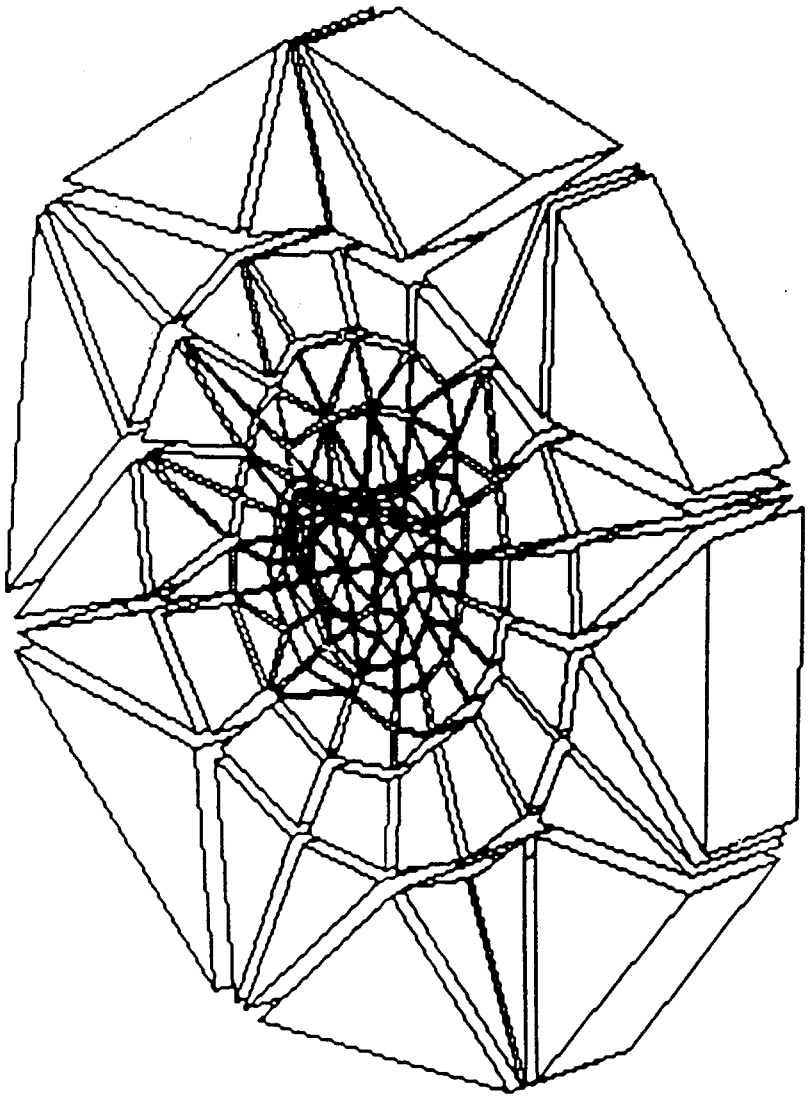

Figure 2. Single three-dimensional, finite-element model layer of the cross section of Figure 1. Each element is shown in its original position but shrunk 15% geometrically to emphasize the element structure.

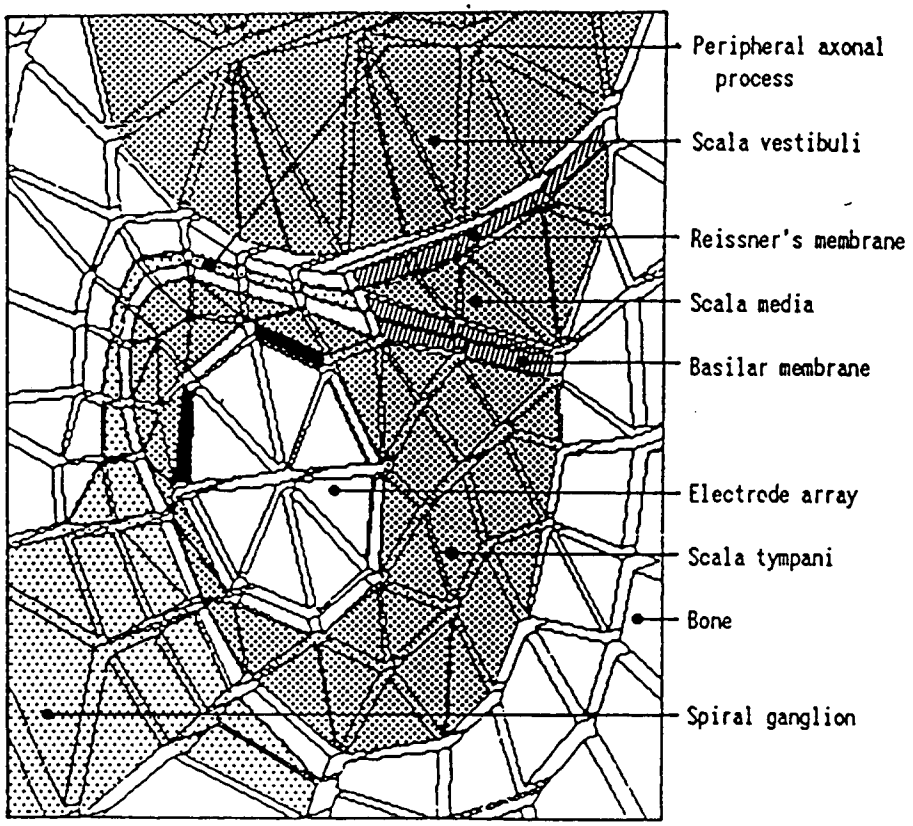

Figure 3. Enlarged view of the central region of the layer of Figure 2, showing the electrode array in scala tympani. Discrete anatomical regions with different resistivities are indicated. Table 1 summarizes the resistivities.

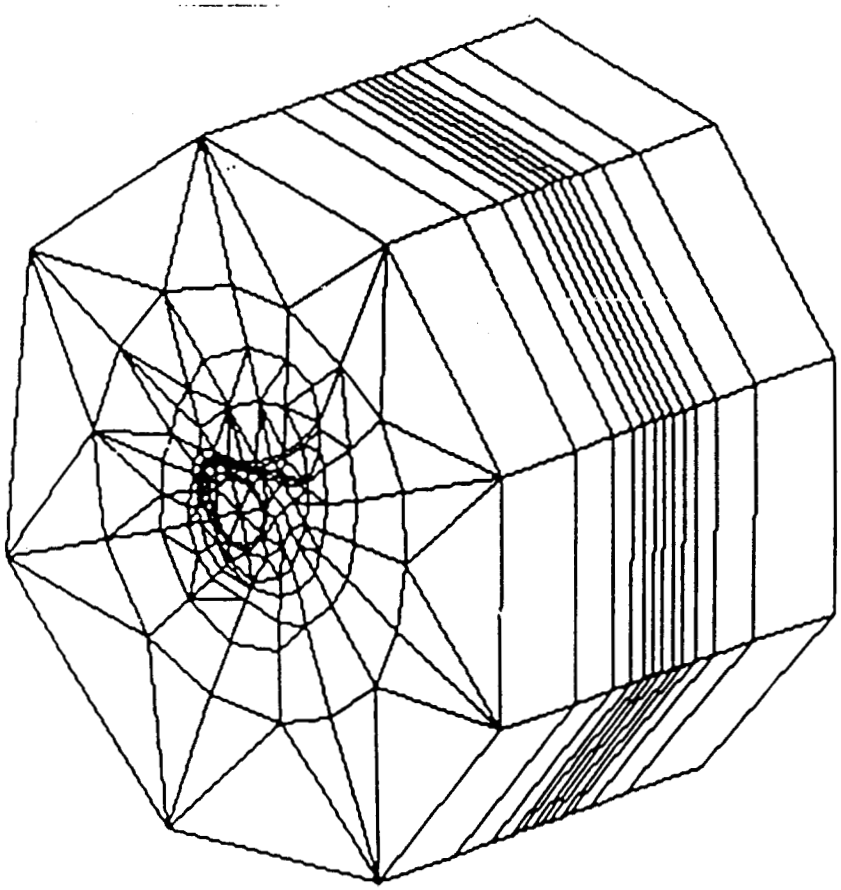

Figure 4. Full three-dimensional model of a straight section of the cochlea. Twelve layers, each similar to the layer shown in Figure 2 but differing in thickness, are assembled along a straight longitudinal axis. Note the higher spatial resolution in the center of the model denoted by smaller element sizes in the cross-sectional view and thinner layers centrally along the longitudinal axis. Figure 5 describes the layer thicknesses.

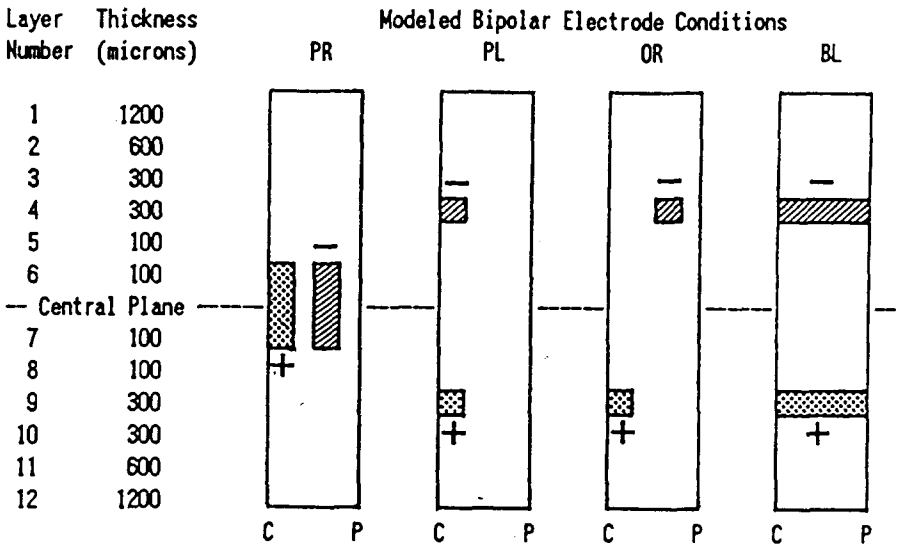

Figure 5. Layer thicknesses and electrode assignments for modeled bipolar electrode conditions. Pure radial (PR), pure longitudinal (PL), offset radial (OR) and banded longitudinal (BL) bipolar electrode configurations are shown as viewed looking down on the electrode assemblies from scala media. Polarity symbols (+ and −) indicate the assigned layers and relative element positions on the electrode insulator assemblies for the positive and negative electrode elements, respectively. Letters, C and P, beneath the electrode assembly outlines indicate the central and peripheral sides of the assemblies, respectively. Layer numbers and thicknesses in microns are indicated. Layer thicknesses are symmetrical about the central plane of the model.

TABLE 1

Regional Resistivities for Finite Element Field Model

Region	Resistivity[1]
Insulator	10^9
Electrode	0.1
Perilymph	70
Endolymph	60
Bone[2]	630
Spiral Ganglion	300
Peripheral Axonal Process	300 axial (anisotropic) 1500 transverse
Reisner's Membrane[3]	60480 (27 Kohm/mm SV to SM)
Basilar Membrane[3]	1800 (2 Kohm/mm SM to ST)

[1] All resistivities are in ohm-cm and are assumed to be isotropic unless otherwise noted.

[2]Based on Spelman [37].

[3] Resistivity selection based on membrane thickness in the finite element model to provide inter-compartmental resistivities between scala media (SM), scala vestibuli (SV) and scala tympani (ST) as measured by Strelioff [38].

modifications of the detailed element structure within scala tympani. Figure 6a shows the electrode array assembly as it would appear if removed from scala tympani. In cross section the electrode array shows an octagonally-shaped core of eight prism elements arranged about a central axis. This central core is specified to be an insulator in all conditions. The outer planes of the prisms are capped with thin, solid, plate-like elements that form the outer surface of the electrode assembly. An electrode configuration is specified by setting resistivities of these surface plate elements to be either insulators or electrode conductors. Node potentials at nodes bordering the conductive electrode surfaces are fixed arbitrarily at +100 or -100 mvolts prior to computation to simulate the electrode potential during stimulation.

Figures 6b through 6e illustrate the selection of surface elements for four different electrode configurations. All views are drawn as if looking toward the right from the modiolus into scala tympani. Figures 6b and 6c represent pure radial bipolar and pure longitudinal bipolar electrode configurations, respectively. Figure 6d is an offset radial configuration that represents the bipolar configuration implemented in the University of California at San Francisco (UCSF) electrode array [20]. Figure 6e shows a banded longitudinal bipolar configuration that represents the adjacent band configuration of the University of Melbourne electrode array [25]. Note that the surface elements selected for the electrodes of the banded longitudinal configuration are selected around the full circumference of the core insulator. The electrode configurations and polarity assignments are summarized in Figures 5 and 6. Table 2 summarizes the electrode widths, electrode assembly diameter and inter-electrode distances.

In addition to the surface configuration of the electrode structure as described above, the diameter and placement of the electrode assembly within the scala also must be specified. Figure 7 shows two scala tympani element structures that model different placements of the electrodes within the scala. Figure 7a shows an 800 micron diameter electrode assembly that is located close to the modiolar wall of scala tympani. This diameter and placement are similar to that of the UCSF electrode array with its mechanical memory [20]. The pure radial, pure longitudinal and offset radial bipolar electrode models use this scala tympani element configuration. Figure 7b shows a 500 micron diameter electrode carrier that is located close to the lateral wall of the scala. This position is consistent with the diameter and placement of the thinner, more flexible Melbourne electrode array in scala tympani [33]. The

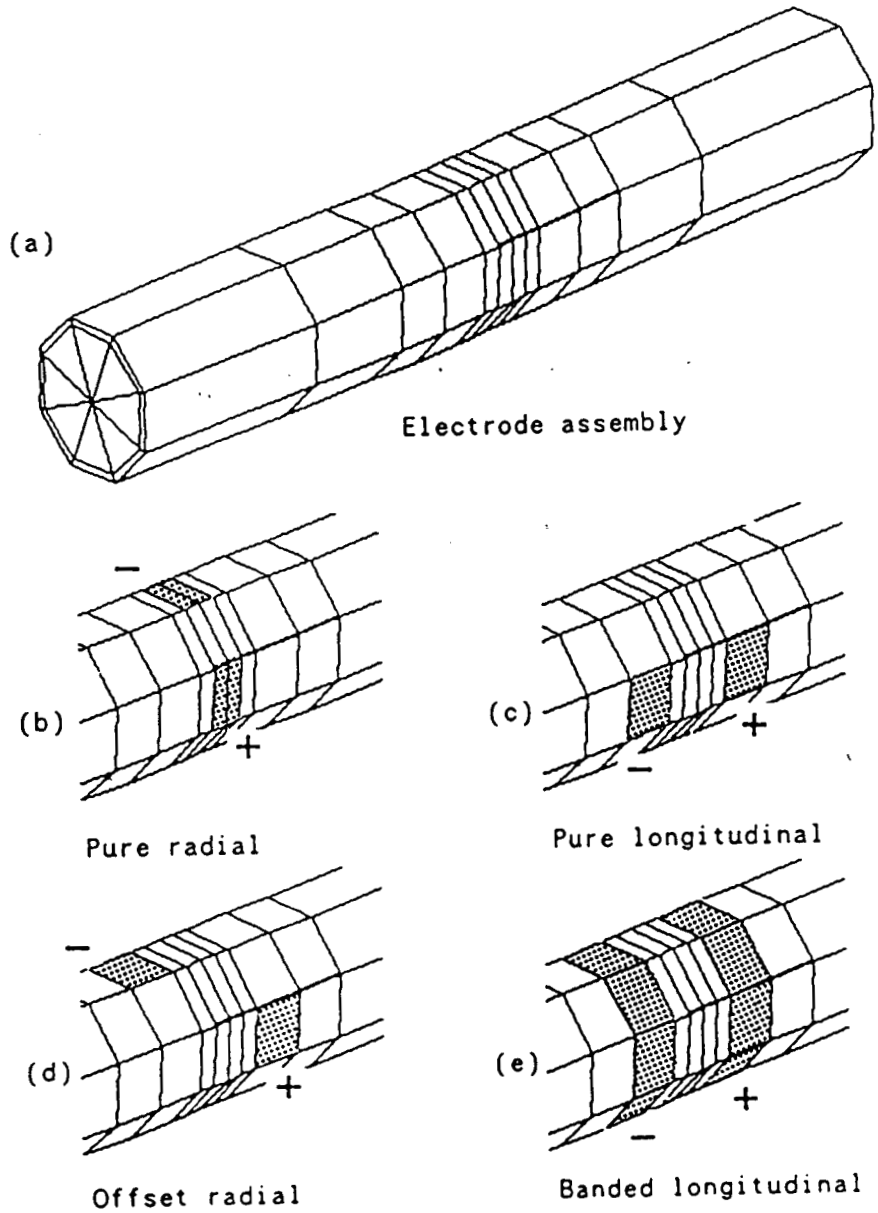

Figure 6. Finite-element model of scala tympani electrode assembly. Panel (a) shows the electrode carrier insulator removed from full model of Figure 4. Panels (b), (c), (d) and (e) indicate the element selection and polarity conventions used for the pure radial, pure longitudinal, offset radial and banded longitudinal bipolar electrode configurations, respectively. Table 2 summarizes the dimensions of these configurations.

Table 2

Electrode Pair Dimensions for Pure Radial(PR), Pure Longitudial(PL), Offset Radial(OR) and Banded Longitudinal(BL) Configurations

	Modeled Bipolar Electrode Conditions			
	PR	PL	OR	BL
Single Electrode Width (microns)	200	300	300	300
Electrode Carrier Diameter[1] (microns)	800	800	800	500
Inter-Electrode Distance[2] (microns)	604	700	924	700

[1] Electrode carrier diameters are maximum diameters of carrier cross sections shown in Figure 6.

[2] Inter-electrode distance is measured between the centers of the electrodes along the surface of the electrode carrier.

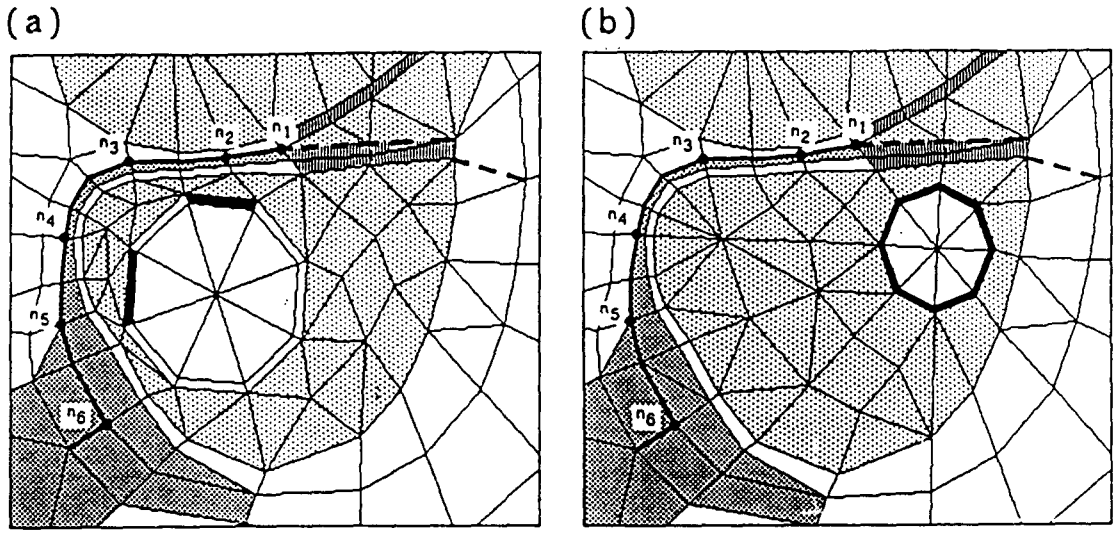

Figure 7. Detailed cross-sectional element structures for the electrode assembly in scala tympani. Panel (a) shows the elements used for the pure radial, pure longitudinal, and offset radial electrode configurations. Panel (b) shows the elements used for the banded longitudinal electrode configuration. The edge of the neural sheet locus is indicated by the broad line. Node positions n_1-n_6 are shown along this locus also. See text for full description.

banded longitudinal bipolar electrode model uses this scala tympani element configuration.

The principal outputs of the model are the potential patterns that occur in the vicinity of the neural elements for fixed potentials applied to the electrodes. To obtain this information, potentials at nodes of elements lying close to the neural track are reported. Figure 7 shows a locus of nodes connected by a broad line that lies along the path of the neural elements. This locus lies on the modiolar side of the peripheral axonal processes and extends from the center of the ganglion region to the habenula. The node locus extends beyond the habenula laterally across the basilar membrane into the bony lateral wall, as shown by the dotted line. Node potentials in this region provide insight into field patterns along the wall of scala tympani. This locus of nodes, as shown in Figure 7, is defined across all layers of the full three-dimensional model, thus forming a generalized locus resembling a curved neural sheet. The spatial dimensions of the neural sheet are thus radial (central to peripheral) along the axes of single individual fibers and longitudinal (basal to apical) across the ensemble of many fibers. Field potential estimates from the model are reported by flattening this neural sheet and examining potential distributions on its surface. Potentials along edges of elements are linear interpolations of the potentials at the nodes that define each edge. Three discrete representations are used to display the potential distribution on the neural sheet. First, isopotential contours are shown on a flattened representation of the neural sheet. Second, specific extracellular potential profiles along the radially-oriented trajectory of selected single neural elements are graphed as a function of position along the fiber. Third, spread function plots show potentials at fixed radial positions along each fiber as a function of longitudinal location of the fiber, indicating relative rates of field decay away from the electrode pair.

C. Potential Field Calculation Results

Pure Radial Configuration

Model predictions for the electrical field patterns of the pure radial bipolar electrode configuration are shown in Figure 8. This calculation is conducted assuming the electrode configuration of Figure 6b with the scala tympani electrode placement of Figure 7a. Figure 8a shows the isopotential contours on the neural sheet described above. Isopotential contours are drawn for potential levels at 5% increments (10 mvolts) of the fixed electrode potentials (plus and minus 100 mvolts). The abscissa is the longitudinal (basal to apical) location along the basilar membrane and the ordinate is the radial (central to peripheral) position along neural fibers in the sheet. Node locations, defining element boundaries, are shown on the neural sheet by crosses. Figure 8a shows two radially-oriented peaks, each indicated by patterns of concentric isocontours, positioned midway along the longitudinal axis. The more centrally located peak is positive in polarity, being closer to the positive electrode near the modiolus. The more radially located peak is negative in polarity. The single, gradually arcing contour that extends along the full extent of the longitudinal axis is the zero potential isocontour.

Also shown in Figure 8a is a grid consisting of solid vertical and dashed horizontal lines. The solid lines indicate selected locations along the model's longitudinal axis that represent the loci of seven fibers lying in the neural sheet. These fiber locations are designated f_1 through f_7 from basal to apical-most. Fiber f_4 lies in the central plane of the model. The symbol associated with each line is used to label plots of data associated with that fiber locus. The dashed horizontal lines indicate six radially positioned loci in the neural sheet that are parallel to the longitudinal axis. These are labeled n_1 through n_6. Position n_1 defines the locus of the habenula. Position n_2 through n_5 define node positions along the peripheral axonal processes of the fibers with approximately 300 micron internodal spacing. Position n_5 lies adjacent to the fiber's cell body on the peripheral side. Position n_6 lies in the center of the ganglion region. Again the symbol associated with each nodal position is used to label plots of associated data.

Potentials profiles for fibers (f_1 through f_7) are plotted as a function

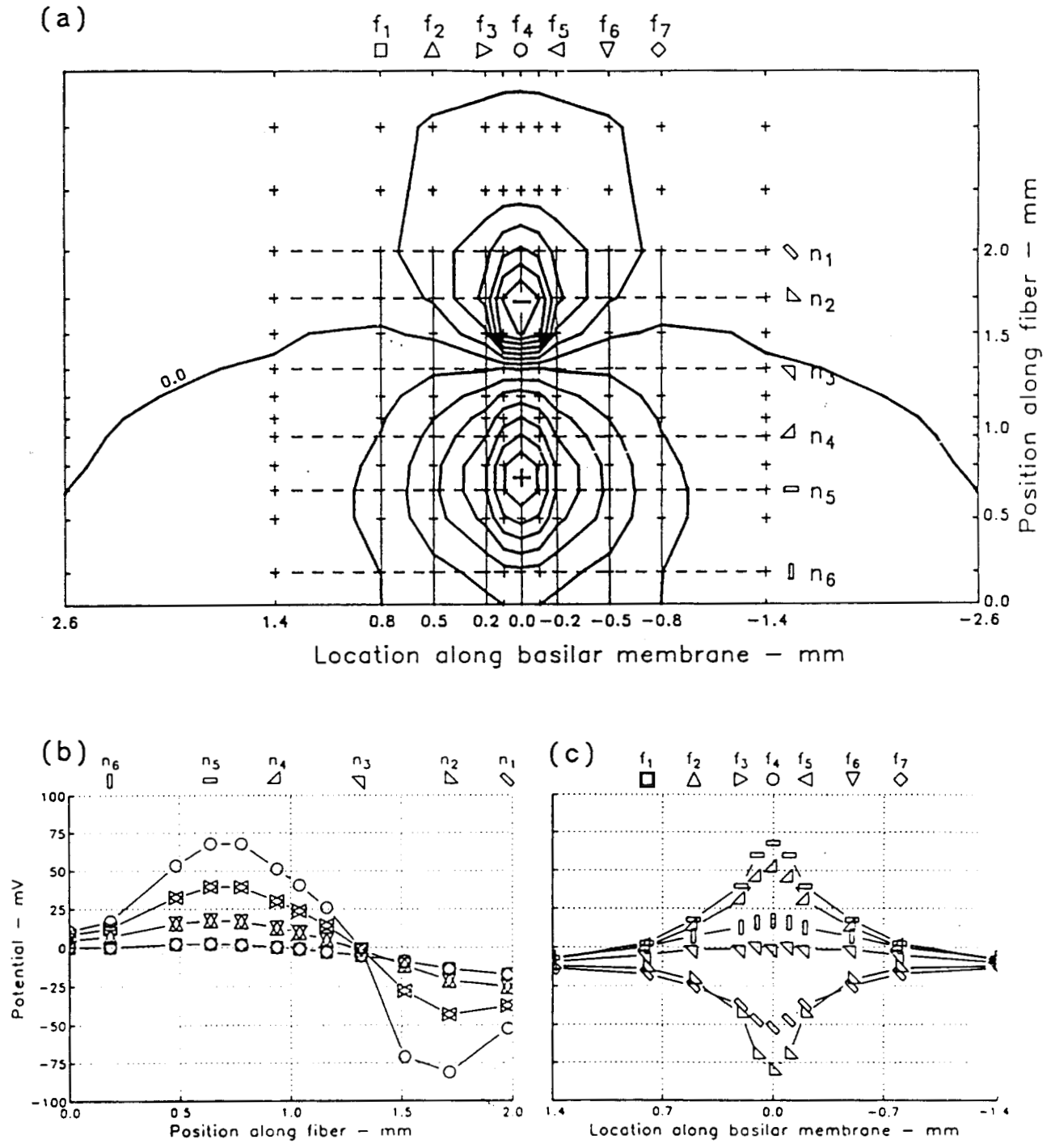

Figure 8. Neural sheet potential patterns for the pure radial bipolar electrode configuration. Panel (a) shows isopotential contours at 10 mvolt intervals for potentials lying on the sheet. The zero potential isocontour is explicitly labeled. Symbols (+ and −) indicate the polarities and the locations of peak potential levels. Panel (b) indicates potential profiles along selected fibers lying in the sheet. Panel (c) indicates the spread of potentials along the longitudinal axis at fixed fiber node positions. See text for full discussion.

of radial position along the fiber in Figure 8b. The greatest peak potential levels and steepest gradients occur along the fibers located closest to the electrode pair (f_3 through f_5). Decreasing peak levels and shallower gradients are seen along fibers located at progressively more distant longitudinal locations (f_1 and f_7). Regardless of its location, each fiber is exposed locally to both positive and negative potentials along its length. The potential spread functions, showing potentials along the longitudinal axis for each nodal position (n_1 through n_6), are shown in Figure 8c for this condition. High absolute peak levels are observed at the midpoint longitudinal location f_4 for both the peripheral most node (n_2) and the node (n_5) adjacent to the cell body. The fields diminish rapidly in the vicinity of the potential peaks. For instance, at the peripheral most node position (n_2), the potential on f_7 is approximately 17 dB below the peak level at the same position on f_4, 800 microns away along the longitudinal axis. At greater longitudinal distances beyond the f_7 location, the potential levels continue to decline.

Pure Longitudinal Configuration

Field patterns for the pure longitudinal configuration are shown in Figure 9. Figures 6c and 7a indicate the electrode configuration and the scala tympani electrode placement used in this calculation. The isopotential contour plot of Figure 9a shows two relative potential peaks of opposite polarity oriented parallel to the longitudinal axis of the model. The maximum potential levels are at node positions n_4 and n_5 along fibers (f_2 and f_6) closest to each electrode. The potential profiles of Figure 9b indicate that each fiber, depending upon its location, is exposed to either wholly positive or negative potentials along its length. Potential gradients are small along the fiber length as compared to the patterns seen for the pure radial configuration. Because of the geometric symmetry of the longitudinal electrode configuration, fibers located midway between the electrode positions (near f_4) receive little or no stimulation. The spread functions of Figure 9c show substantial potential spread along the longitudinal axis. At a location (f_7) 800 microns longitudinally from the central plane of the model, the potential level at node position n_5 is at most 5 dB below the peak level occurring at f_6. Potentials at more distant longitudinal locations along the same nodal locus continue to decline.

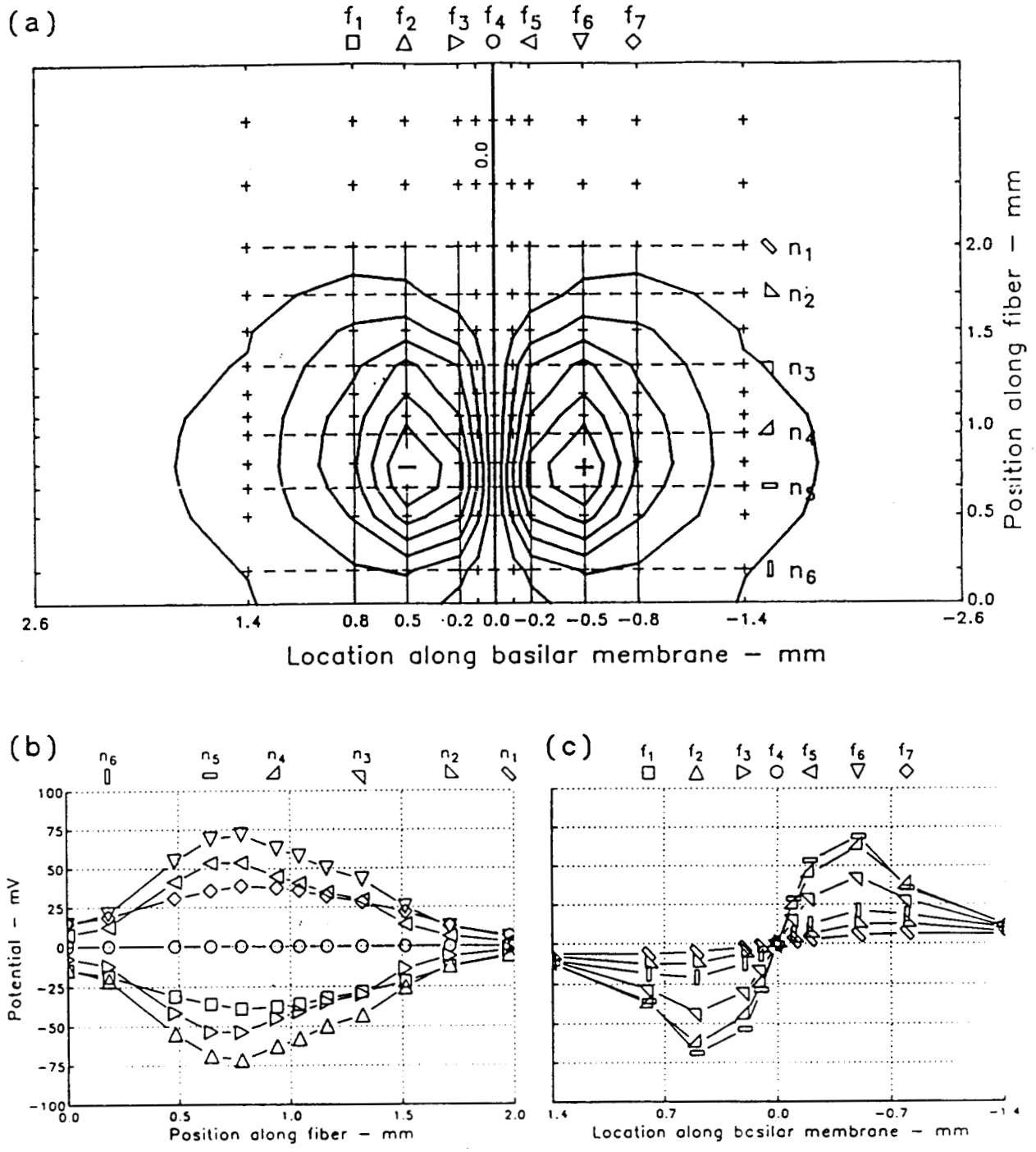

Figure 9. Neural sheet potential patterns for the pure longitudinal bipolar electrode configuration. Panel (a) shows isopotential contours at 10 mvolt intervals for potentials lying on the sheet. The zero potential isocontour is explicitly labeled. Symbols (+ and -) indicate the polarities and the locations of peak potential levels. Panel (b) indicates potential profiles along selected fibers lying in the sheet. Panel (c) indicates the spread of potentials along the longitudinal axis at fixed fiber node positions. See text for full discussion.

Offset Radial Configuration

The offset radial bipolar configuration is a combination of the pure longitudinal and pure radial bipolar configurations. Figure 10 shows the model field predictions based on the electrode configuration of Figure 6d and the scala tympani placement shown in Figure 7a. The isopotential contour plot shows a more complicated pattern than seen before. Again two relative potential peaks are observed that are offset in radial position and longitudinal location (Figure 10a). The fiber potential profiles of Figure 10b reveal a heterogeneous pattern of stimulation that varies dramatically as a function of fiber longitudinal location. Fibers located near the positive, apical electrode (f_5 and f_6) have profiles almost identical to those seen with the pure longitudinal configuration. High peak values with relatively small gradients are observed with positive potentials along almost the entirety of the peripheral fiber process. Peak levels for these fibers are near the cell body at node position n_5. In contrast, potential profiles for fibers located near the negative, basal electrode (f_2 and f_3) have high peak negative potentials with steep gradients occurring at the more peripheral end of the fiber (n_2). At more central positions along these fibers (n_4 through n_6) the extracellular potentials approach zero. Fibers located near the central plane of the model (near f_4) are exposed to low peak stimulus levels of both polarities with relatively shallow gradients. The spread function (Figure 10c) for the offset radial longitudinal configuration shows a pattern of field decay similar to that of the pure longitudinal configuration. On fiber f_7, 800 microns longitudinally from the central plane, potential levels at node position n_5 are about 7dB below peak levels. Potentials at this node position continue to decline at more distant longitudinal locations.

Banded Longitudinal Configuration

The banded longitudinal bipolar electrode configuration produces a fundamentally different field pattern from those previously discussed. The electrode configuration of Figure 6e and the scala tympani placement of Figure 7b are used. Figure 11a shows the isopotential contours. Two longitudinally-oriented peaks are present in the region of the basilar membrane, radially beyond the most peripheral extent of the fibers (n_1). This

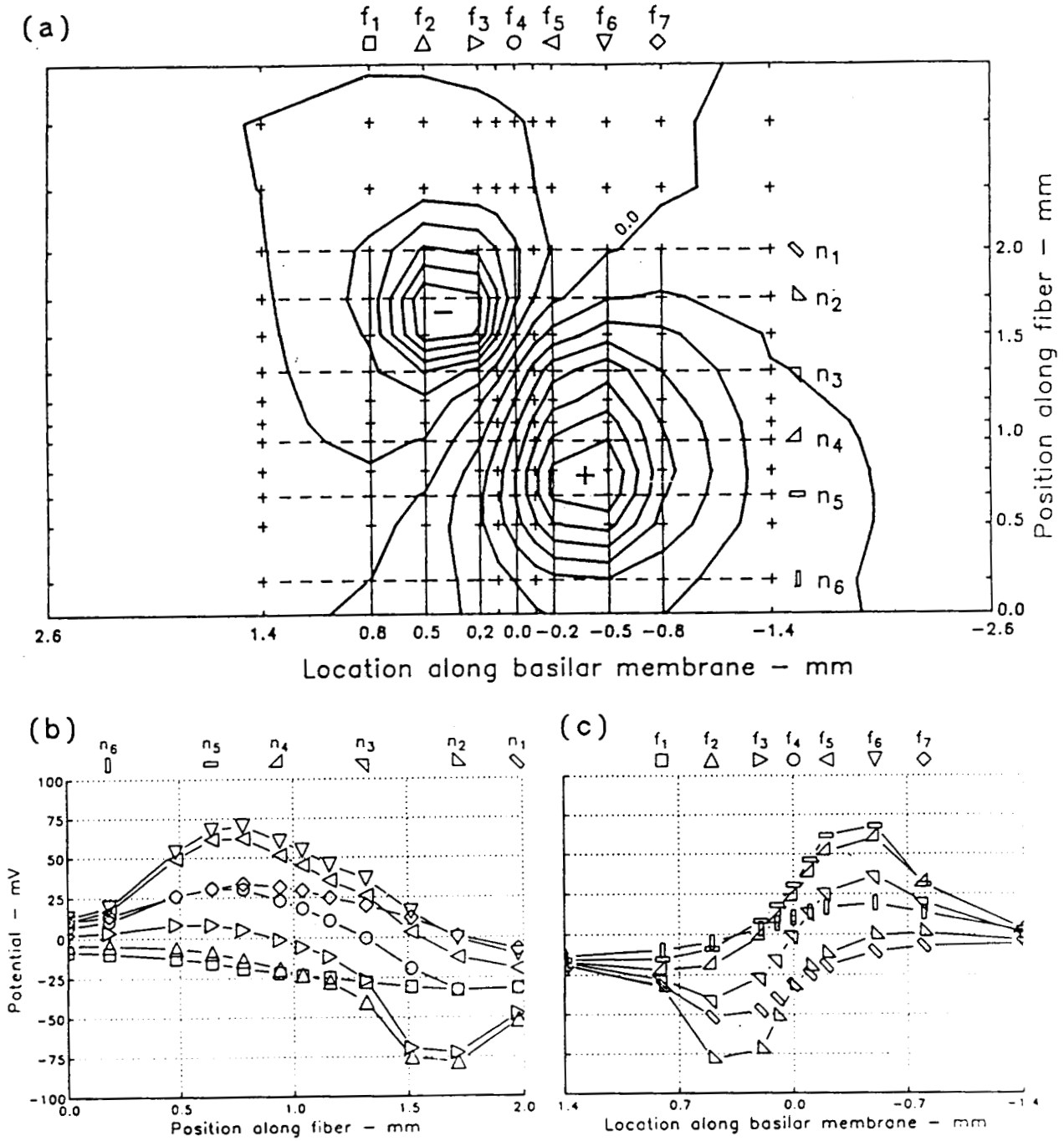

Figure 10. Neural sheet potential patterns for the offset radial bipolar electrode configuration. Panel (a) shows isopotential contours at 10 mvolt intervals for potentials lying on the sheet. The zero potential isocontour is explicitly labeled. Symbols (+ and −) indicate the polarities and the locations of peak potential levels. Panel (b) indicates potential profiles along selected fibers lying in the sheet. Panel (c) indicates the spread of potentials along the longitudinal axis at fixed fiber node positions. See text for full discussion.

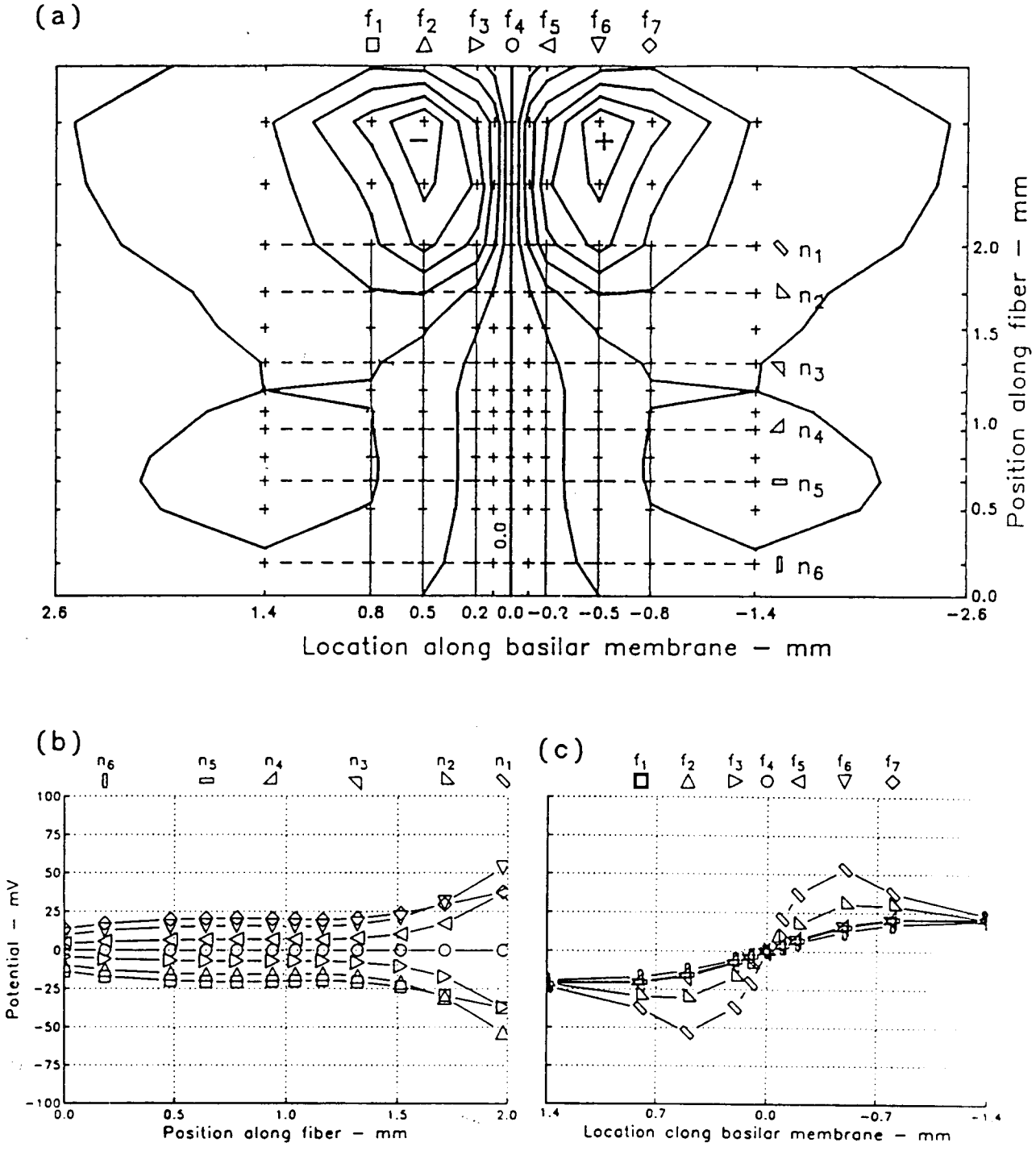

Figure 11. Neural sheet potential patterns for the banded longitudinal bipolar electrode configuration. Panel (a) shows isopotential contours at 10 mvolt intervals for potentials lying on the sheet. The zero potential isocontour is explicitly labeled. Symbols (+ and −) indicate the polarities and the locations of peak potential levels. Panel (b) indicates potential profiles along selected fibers lying in the sheet. Panel (c) indicates the spread of potentials along the longitudinal axis at fixed fiber node positions. See text for full discussion.

is a consequence of the peripheral placement of the electrode carrier within scala tympani. The fiber potential profiles of Figure 11b reveal a field pattern of single polarity, almost constant, low amplitude potential levels along the fiber. Only at the most peripheral end (n_1) of some of the fibers are significant gradients present. The spread functions in Figure 11c show a remarkably homogeneous pattern of a broadly spreading field of potential. At the 800 micron longitudinal location (f_7), field levels at node positions n_3 through n_5 are only beginning to reach a maximum, indicative of a broadly spreading field pattern. The one exception to this pattern is the spread function computed for the most peripheral fiber positions (n_1). Here a relative peak is observed near 500 microns longitudinally on f_6, decreasing by 3.2 dB at the 800 micron location of f_7.

D. Limitations of the Field Model

In addition to the limiting assumptions previously outlined for setting up the model, two more limitations emerge from examination of the neural sheet potential patterns. First, the model is spatially limited in total length and element resolution along the longitudinal axis. This is particularly evident in the case of the banded longitudinal electrode configuration. One design goal of the model was to provide fine spatial resolution in the central region surrounded by progressively larger elements (hence lower resolution) toward the model boundary. This structural organization minimizes the model's node and element count and leads to more efficient calculations with smaller memory requirements. Generally, such a configuration would be adequate for modeling the spatially constrained field patterns of bipolar electrode pairs located in the central region of the model. The broadly spreading fields of monopolar electrodes [9] cannot be calculated accurately in the present model and thus are not addressed in this report. For the present model the pure radial, pure longitudinal and offset radial electrode pair field patterns are reasonably modeled. However, in the case of the banded longitudinal configuration, the spread of the electrical fields is unexpectedly large. Here the total length and relatively coarse resolution of the elements along the longitudinal axis of the model may produce distorted longitudinal field estimates. The relative degree of distortion is not presently known but may be examined by adding elements to expand the model longitudinally and then computing the fields

again. Lengthening the model, however, will further distort the field estimates from those existing in an intact cochlea, since cochlear spiral curvature is not addressed in the present model. A second limitation of the field model is that additional anatomical detail needs to be modeled in particular regions of the cochlea. One region is the lateral wall of scala tympani, which should be described as the soft tissue structure of the stria vascularis and the spiral ligament, instead of the presently modeled bone. Another region requiring refinement is the modiolus. Here anisotropic tracts of fibers from higher cochlear turns are missing, as well as details of the axons coursing centrally from neuronal cell bodies lying in the spiral ganglion near the electrodes. Detailing the modiolus is particularly important since the calculated potentials indicate that axons of fibers projecting centrally off of the edge of the neural sheet are still in the presence of significant extracellular fields. To model the response of a neuron to electrical stimulation, it is most important to model all surfaces of the neuron that are exposed to non-zero extracellular fields and thus are passing current. For instance, anodic currents entering a fiber near an anode stimulate a neuron by activation of sites remote to the anode as current passes out of the cell [27].

To explore how the predicted extracellular potential fields influence the firing probability of the neural fibers, we turn to the neural component of the integrated field-neuron model.

E. Neural Responsiveness to Extracellular Fields

A variety of lumped element models have been proposed to describe the response of myelinated nerve fibers to extracellular potential fields. All of these models are extensions of the original work of McNeal [21] for predicting the subthreshold behavior of a myelinated neuron in an electrical field. McNeal's model describes an electrical network of the distributed myelin and nodal membrane characteristics of an infinitely long myelinated fiber. Node behavior is described by the Frankenhauser-Huxley equations [8]. Such a model is capable of predicting the occurrence of an initial spike from a resting state. Enhanced versions of this model have been described for computing suprathreshold and repeated spiking behavior [6,30]. Similar models have been developed to describe the behavior of intracochlear fibers during

electrical stimulation [5, 6].

Rattay [28, 29] has shown that the responsiveness from a resting state of both myelinated and unmyelinated infinitely long fibers in electrical fields depends on the second spatial derivative of the field in the extracellular medium. He defines an activating function which for myelinated fibers is the second difference quotient of the extracellular potential field when sampled at node positions along the fiber. Biophysically, the activating function at a particular node is proportional to the summation of intraaxonal longitudinal currents at the node position. At rest this current summation is zero; however, during exposure to extracellular fields, the net longitudinal current flow at a node position may be either positive or negative. This field-induced net summation current flows across the nodal membrane in addition to the resting state nodal currents. A positive activating function value correlates with a positive outward current at the node, leading to nodal depolarization. A negative activation function value corresponds to nodal hyperpolarization. The greater the absolute magnitude of the activating function, the greater the local effect at the node.

As an initial examination of the responsiveness of neural fibers to the predicted electrical fields, we compute the activating functions for the set of neurons whose potential profiles were described above. Here we assume that no cell bodies are present and that the fibers are infinitely long and of uniform diameter with the previously described node spacing. Activating function predictions are independent of fiber diameter. The activating functions are computed for the four node positions (n_2 through n_5) along the peripheral axonal process from the edge of Rosenthal's canal (n_5) to the node position (n_2) adjacent to, but not including, the habenula (n_1). End effects due to fibers terminating at the habenula are not specially treated. Fiber termination regions are probably specific stimulation sites for neurons in electrical fields [31], a result that would not appreciably change the neuronal behavior predicted by this present analysis. In Figures 12 - 15, activating function values are plotted for each of the modeled electrode configurations for each node both as a function of node position along the fiber (panel a of each figure) and as a function of fiber location along the basilar membrane (panel b of each figure). The functions are calculated assuming a positive current stimulus applied to the modeled electrode configurations and using the polarity conventions described in Figures 6 and 8-11. A reversal of stimulus polarity at the electrodes reverses the field

polarity, but conserves its basic shape; hence, with a negative stimulus applied, a negative activating function value signifies depolarization of the node.

This analysis of neuronal responsiveness is useful only for identifying the probability that a node will initiate a neural spike in response to a monophasic pulsatile stimulus. By definition the activating function assumes the neuron is at resting state, so the measure indicates only the direction and degree of tendency of the node to change from quiescence. No temporal integration behavior is included. Similarly, while the possible occurrence of anodic blocking can be noted, such phenomena cannot be demonstrated.

It is important to emphasize that the present analysis assumes the presence of myelinated fibers extending from the habenula centrally. This is more often not the case in the implanted, deafened cochlea [10, 17, 18]. Extensive loss of complete auditory afferents often occurs. When the fiber is present, the peripheral axonal process may not be present. When the peripheral process is absent, the target element for electrical stimulation probably consists only of the cell body and its centrally projecting axon. For fibers in this condition, the activating function calculations have little relevance. The present model addresses field patterns and neuronal responsiveness only in the region of the peripheral axonal process. Despite this limitation, it is worth pursuing this analysis to gain insight into the general principles of intracochlear electrical stimulation and to understand the results of experimental studies of intact cochleae.

Pure Radial Configuration

Activating function predictions of neuronal responsiveness are now considered for the pure radial electrode configuration with a positive monophasic stimulus (cathode lateral). In Figure 12a the largest activating function value occurs at the most peripheral node (n_2) of the fiber closest to the electrode pair (f_4). Actually node position n_2 is the only position that would be stimulated for any given fiber in the target field for this polarity stimulus since the activating function is positive only at this position. It is important to note that in this cathode lateral condition, more centrally positioned nodes (n_3 through n_5) are hyperpolarized, raising the possibility of anodal blockage. In Figure 12b the magnitude of the activating function for node n_2 diminishes rapidly (-40dB/mm between f_4 and f_5) as a function of

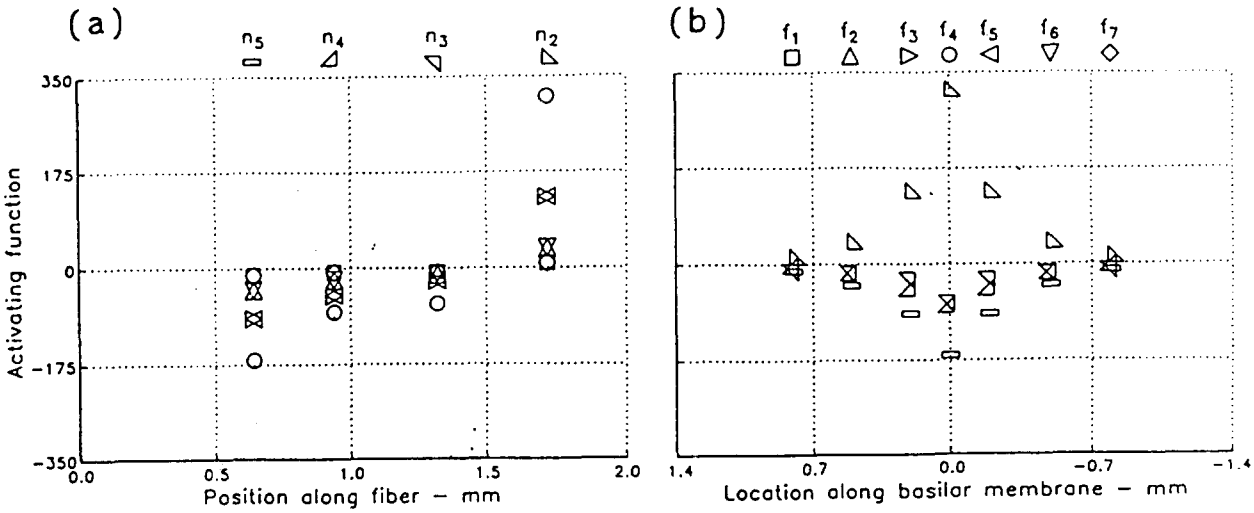

Figure 12. Fiber activating function plots for the pure radial bipolar electrode configuration as a function of nodal position along fibers (a) and of location of a fiber along the basilar membrane (b).

longitudinal fiber location. Assuming that a high activating function value correlates with low fiber threshold, very high thresholds would be expected at all locations within the cochlea except near the radial pair location. Here a sharp decrease in threshold would occur, forming a sharp, symmetrical threshold dip centered at the electrode pair location. This is precisely the single unit threshold behavior that has been observed by van den Honert and Stypulkowski (Figure 6 of [11]) in the cat using a radial bipolar electrode pair for electrical stimulation in an acoustically intact ear. They monitored fiber electrical threshold and measured acoustic characteristic frequency to establish each fiber's location along basilar membrane. The variability between animals in their data is most likely due to uncertainties in scala tympani electrode placement.

For a negative stimulus polarity (cathode medial) applied to the same electrode configuration, the model predicts stimulation of a completely different set of nodes. In this case, the most strongly depolarizing node (signified now by the maximum negative activating function value) again lies along fiber f_4 but is now the most centrally positioned node n_5. This central node (n_5) is driven only about half as much under cathode medial conditions as the most peripheral node (n_2) on the same fiber with the cathode lateral. The two adjacent, but more peripherally positioned, nodes (n_3 and n_4) are also

activated but to a lesser degree. Looking across the ensemble of fibers, we see again a diminishing depolarization drive for fibers more distant from the electrode pair (-27 dB/mm between f_4 and f_5). In both polarity conditions, the widths of the target fields of depolarized fibers along basilar membrane are the same. Predictions of unit thresholds versus fiber location for the cathode medial condition would provide a similar picture of a sharp threshold dip centered at the electrode location, with two qualifications: (1) with the cathode lateral, the depth of the threshold dip should be less pronounced, and (2) the maximum width of the dip should be the same in both conditions. This again is consistent with observed unit data (Figure 6 of [11]).

Pure Longitudinal Configuration

The predicted neural response patterns for the pure longitudinal bipolar configuration are quite different. For a positive monophasic stimulus (cathode basal), Figure 13a shows the largest positive activating function (hence depolarizing) values located at central node positions (n_5). Figure 13b indicates that these nodes lie along fibers (f_2 and f_3) nearest the more basal electrode. In contrast, fibers located near the more apical, anodic electrode (f_5 and f_6) are only moderately stimulated at the most peripheral nodes (n_2) but are strongly hyperpolarized at the most central nodes (n_5). A plot of predicted fiber thresholds versus basilar membrane location would show high thresholds everywhere across the cochlea except in the vicinity of the electrode pair. Near the electrode pair two threshold dips would be expected. One dip, near the basal cathode and including fibers f_2 and f_3, would be relatively deep, but not as deep as the dip seen with the pure radial, medial cathode configuration. The width of this dip should be approximately half that for the pure radial configuration. Midway between the electrodes the thresholds should rise to high values. Near the apical anode, including fiber locations f_5 and f_6, another dip is expected that would be even shallower in depth. For fibers in this region anodal blockage is a possibility since more centrally positioned nodes are hyperpolarized. A negative monophasic (cathode apical) stimulus would produce a similar distribution with the anodic and cathodic threshold dips reversed in position. Van den Honert and Stypulkowski observed this pattern in experiments with longitudinal bipolar electrodes [11]. In their report the cathode basal condition demonstrates a modest threshold dip near the anode, whereas a very narrow, deeper threshold dip

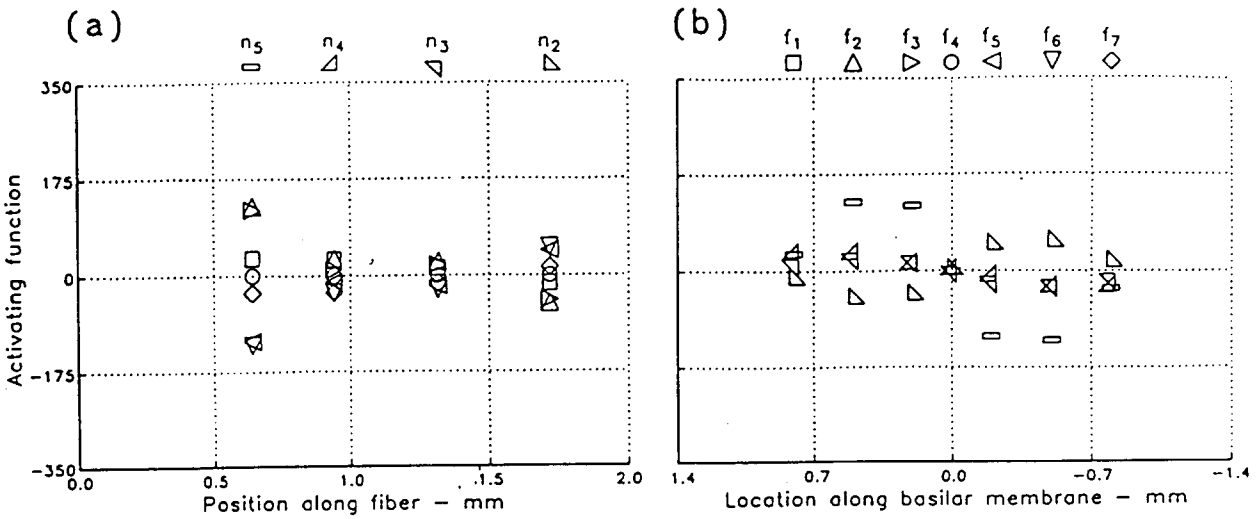

Figure 13. Fiber activating function plots for the pure longitudinal bipolar electrode configuration as a function of nodal position along fibers (a) and of location of a fiber along the basilar membrane (b).

occurs near the cathode for the anode basal condition (Figure 5 of [11]). Insufficient unit data from the basal cochlea prevented a full demonstration of the bimodal threshold distribution. Our present model fails to predict the small, but broadly distributed decrease in thresholds they observed when the cathode was most apical. We interpret that decline as due to the influence of the apically positioned cathode on fibers from apical regions of the cochlea passing through the modiolus. Because van den Honert and Stypulkowski's electrode was inserted only about 5 mm into the first turn, the more basal electrode of the longitudinal pair was substantially further away and somewhat shielded by the apical electrode from the core of the modiolus. Only when the cathode is apically located could it influence the modiolus. This geometry is not described by the present field model.

Offset Radial Configuration

The neural response patterns for the offset radial configuration are similar to the pure radial configuration for node site selection but more closely resemble the pure longitudinal configuration in fiber distribution. For a positive monophasic stimulus (cathode more basally and peripherally located), the depolarized nodes are those only at the most peripheral node

position n_2, as shown in Figure 14a. This pattern is very similar to that computed for the pure radial configuration (Figure 12a). Figure 14b indicates that the most strongly depolarized node sites are on fibers f_2 and f_3 near the cathodic electrode. Fibers near the central plane (f_4) and near the anodic electrode (f_5 and f_6) are also depolarized at the n_2 node position. These fibers are hyperpolarized at more central node positions, however, raising the possibility of anodal blockage. In contrast, for a negative monophasic stimulus (cathode more apical and central), the depolarized nodes will be those closer to the ganglion at position n_5 and lie on fibers f_5 and f_6 near the cathode. In this case, the field of excitation is substantially smaller in extent along the basilar membrane than with a positive monophasic stimulus. There are no VIII nerve single unit studies of fiber thresholds using an offset radial electrode pair for stimulation. Merzenich and White [22] recorded unit thresholds in the central nucleus of the inferior colliculus of cat while electrically stimulating with pure radial, pure longitudinal and offset radial electrode configurations. They acoustically stimulated the contralateral ear to determine characteristic frequencies, taking advantage of the binaural organization of the central nucleus. Although limited in the number of animals, their results suggest an ordering of unit thresholds based on electrode configuration. All three configurations stimulated a narrow region of the cochlea with pure radial being most selective. They found that collicular unit thresholds were either low, intermediate, or high, depending on whether the electrode configuration was offset radial, pure longitudinal or pure radial, respectively. This ordering is exactly opposite the order expected from the model threshold predictions for these configurations. This ordering however is consistent with the ordering of the expected ensemble widths, and hence the number of fibers, for each stimulus configuration. Interpretation of these results is problematic. The relationship between central nucleus thresholds and cochlear fiber activity is not well understood, particularly with regard to how intermediate neuronal pathways process temporally and spatially complex activity, occurring across an ensemble of peripheral fibers. Also, this study recorded thresholds using continuous sine wave stimuli instead of the single monophasic pulses of our model. While the binaural, collicular recording method may provide useful estimates of fiber place, especially in deafened ears, interpretation of collicular unit threshold levels in terms of peripheral stimulation mechanisms should be questioned, until their validity is confirmed experimentally.

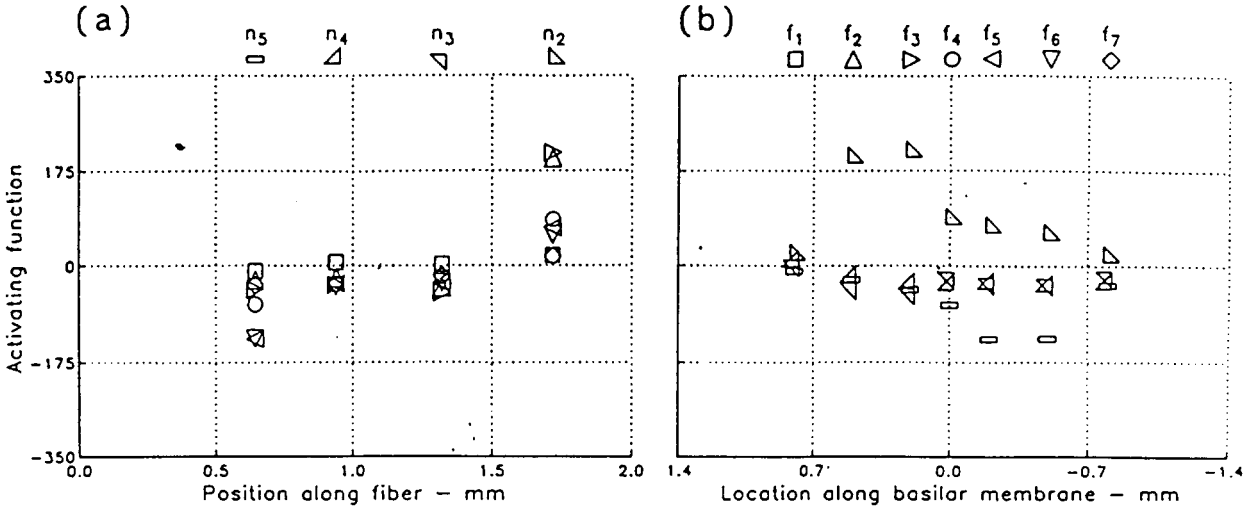

Figure 14. Fiber activating function plots for the offset radial bipolar electrode configuration as a function of nodal position along fibers (a) and of location of a fiber along the basilar membrane (b).

Banded Longitudinal Configuration

The neural activation pattern for the banded longitudinal configuration shown in Figure 15 deviates from the patterns previously described. Here the activating functions for positive monophasic stimulation predict very small depolarization at the most peripheral node positions (n_2 and n_3) of fibers f_5 and f_6 lying near the cathodic electrode band. Node n_3 on fiber f_7 is slightly depolarized also. Near the anodic electrode band the field is symmetric, but opposite in effect, where the most peripheral nodes (n_2 and n_3) are hyperpolarized along fibers f_2 and f_3. With negative monophasic stimulation a similar pattern of nodal stimulation occurs, however now with the cathodic and anodic band positions reversed. Taken to their logical conclusion, these activating function patterns suggest that stimulation with the banded longitudinal electrode pair would exhibit a very high threshold for neural response. In addition, in the case of pathological loss of the peripheral process, the threshold would jump to exceedingly high values. These predictions are clearly not in agreement with extensive clinical

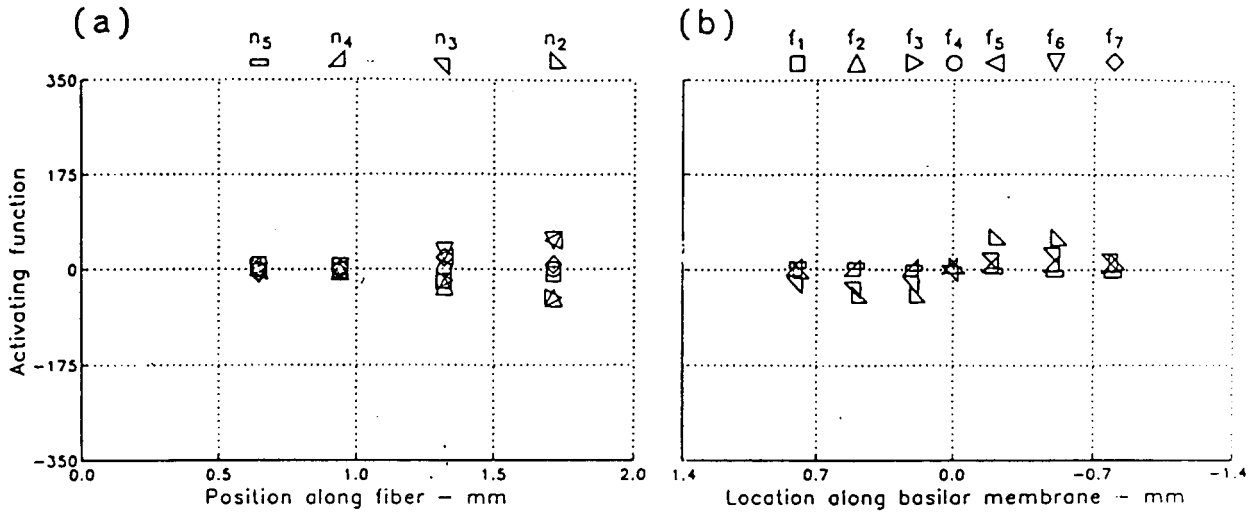

Figure 15. Fiber activating function plots for the banded longitudinal bipolar electrode configuration as a function of nodal position along fibers (a) and of location of a fiber along the basilar membrane (b).

experience using the Melbourne implant system. It is possible that the primary nodes of neural stimulation are located more centrally, perhaps near the cell body or along the centrally projecting axons. Indeed, this possibility cannot be ruled out with regard to the other configurations discussed as well. As discussed earlier, expansions of the model are planned to better describe field patterns in the modiolus. The banded longitudinal configuration, however, as described here, produces a broadly spreading field that stimulates a wider distribution of fibers than would be expected for the pure radial, pure longitudinal or offset radial configurations. The extent of this difference is not yet fully determined.

F. Improvements to the Neural Model

Analysis of neuronal responsiveness using activating functions is at best simplistic. There are numerous aspects of neuronal anatomy and physiology that are not addressed by this analysis which only predicts initial sites of excitation along uniform myelinated fibers. No insight into behavior involving temporal integration of membrane currents or multiple spike firing is provided. Anatomical variability due to pathological loss of peripheral processes and the presence of the cell body are not accounted for. To address these limitations, an expanded, anatomically and physiologically-based neural model of electrical stimulation has been developed.

The expanded model extends the work with the previous neural models [5, 21, 29, 30] by including the electrical impedance of myelin, by incorporating mammalian node characteristics, and by allowing for geometric scaling to account for varying anatomical dimensions. A portion of this model is presented in Figure 16. The neuron model comprises a section of a myelinated axon containing 19 active nodes of Ranvier. Each node is isolated from adjacent nodes by 9 myelinated segments. The ends of the neuron consist of 9 myelinated segments terminating in a sealed membrane. In all 199 computational segments are included in the model. Nodes of Ranvier are located at segments 10, 20, ..., 180, 190. The myelin segments are assumed to be passive and comprise simply a parallel combination of the transmembrane capacity and resistivity. Each myelinated segment is specified by the geometric dimensions of the segment (i.e., radius, length, myelin thickness). The lumped-element electrical properties are then computed assuming a cylindrical model of the segment and using specific tissue characteristics (i.e., axoplasm and myelin resistivities and myelin dielectric constant). Each node is described electrically by a transmembrane capacity in parallel with both a voltage-controlled current source and a series combination of a leakage resistance and a fixed voltage source. The behavior of the current source is described by Frankenhauser-Huxley type equations in the present configuration. Future versions will use Hodgkin-Huxley type equations adjusted for mammalian node characteristics [40]. Transmembrane capacity and leakage resistances are calculated in a manner similar to the passive properties of the myelinated segments. The battery sources are adjusted to provide the normal resting membrane potential for the cell at each of the active nodes. External to the axon at each segment is a voltage source, which

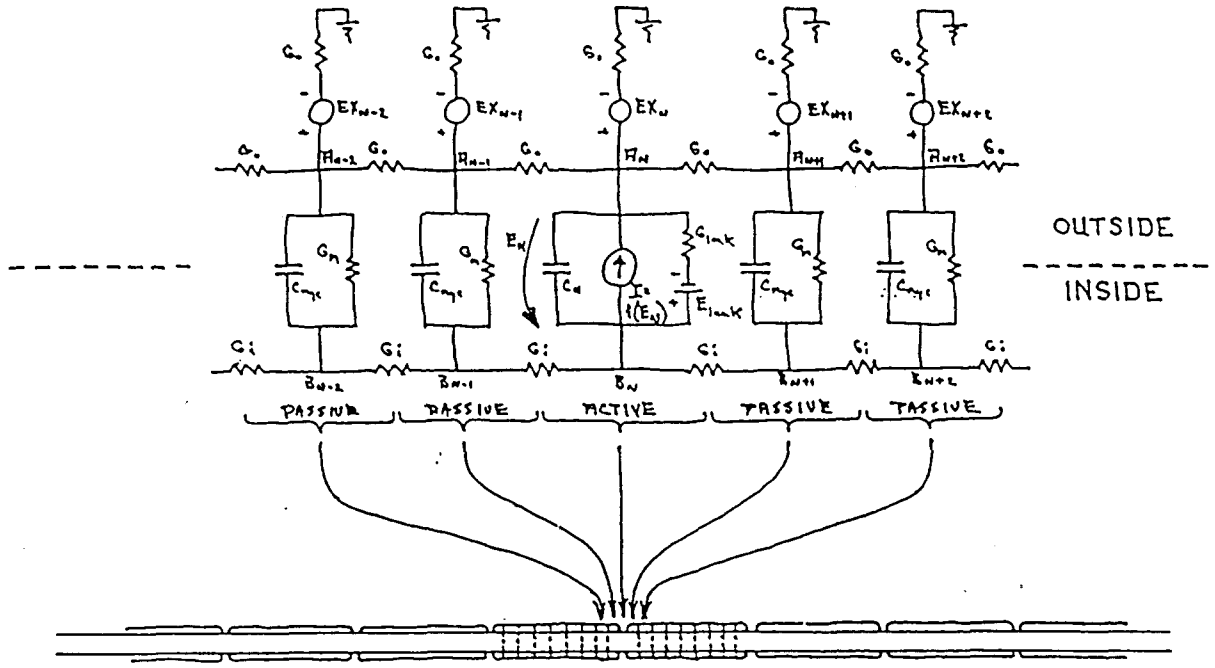

Figure 16. Lumped-element model of a myelinated neuron stimulated by an extracellular electrical field. See text for full description.

drives through the impedance of the extracellular medium. These external voltage sources are set to define the extracellular potential along the cell. Cell body characteristics are incorporated by varying the length and diameter of the myelinated segments between two nodes so as to approximate the longitudinal cross-sectional profile of the cell body in a step-wise manner. At present the model is solved iteratively using Euler approximations for the differential equations and fixed time steps (1.0 usec).

While work with this model is in a preliminary stage, an early result illustrates the significance of the cell body in neural responsiveness to electrical stimulation. Consider the response of a single 1.0 micron diameter myelinated fiber with 250 micron internodal spacing to a step-function extracellular voltage stimulus. The stimulus potential profile along the fiber is an idealized version of the field expected for a pure radial electrode configuration and is shown in the upper panels of Figure 17. This field profile spans a distance of two internodal lengths between peak anodic and cathodic levels. The lower portion of Figure 17a shows the transmembrane potentials for each computational segment along a short section of the fiber, sampled at 40 usec. time intervals. The results indicate that the maximal

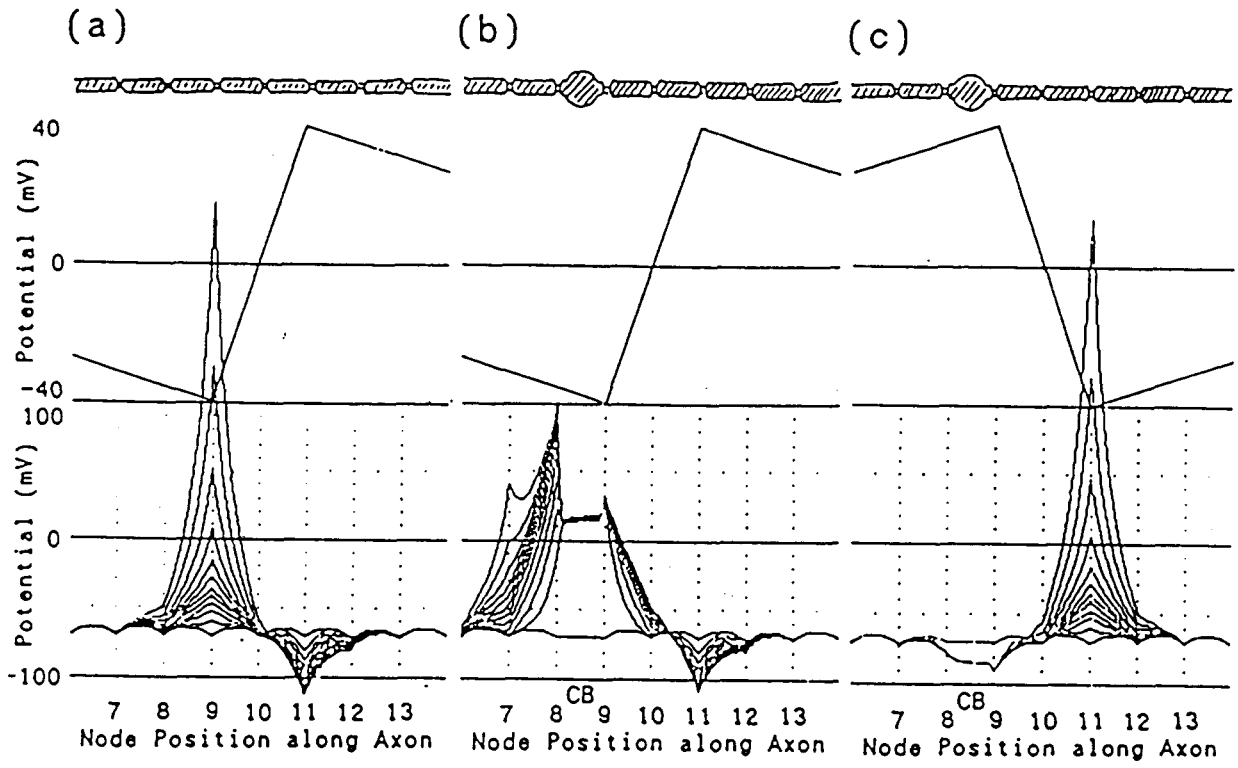

igure 17. Neural model transmembrane potentials as a function of position along the axon in response to extracellular stimulation. Potentials are plotted at rest condition and at every 40 usec. after application of a step-function extracellular field. The field profile along the fiber is shown in the central portion of each panel. The upper portion of each panel describes the anatomical configuration of the modeled neural element. Panel (a) shows the response of a constant diameter fiber to a field profile that is maximally cathodic at node position 9 and maximally anodic at node position 11. Panel (b) shows the response of the same fiber with a cell body included between node positions 8 and 9 to the same electrical field. Panel (c) shows the response to the same neural element of panel (b) but with the polarity of the extracellular field reversed.

depolarization of the fiber occurs at the node (9) nearest the peak cathodic region of the stimulus field. This also is the site that activating function analysis would predict for initial depolarization. Hyperpolarization occurs maximally at the node (11) nearest the peak anodic region. The response in Figure 17b is computed with an identical stimulus condition, except a myelinated, egg-shaped cell body (20 micron diameter and 30 micron length) has been introduced between node positions 8 and 9. This cell body position relative to the potential profile peaks was chosen to approximate the potential profile distribution computed for the pure radial bipolar electrode configuration of Figure 8. Termination of the modeled fiber at the habenula has not been considered in this analysis. The modeled neuron's response is dramatically affected by the cell body presence. Node 9 is no longer the principal node of activation. Now node 8, on the opposite side of the cell body, is depolarized the most. Note also that node 7 is depolarizing rapidly as well, giving rise to an action potential propagating centrally along the axon. In the vicinity of node 11, the hyperpolarization pattern is very similar to the pattern generated without the cell body present (Figure 17a). The model conditions for Figure 17c are similar to the conditions for Figure 17b, with the only change being a reversal of stimulus polarity. Node 11 is now nearest the peak cathodic region and is depolarized the most. Nodes 8 and 9 are hyperpolarized along with the cell body region of the fiber. The depolarization pattern at node 11 is similar to what would be expected for the uniform fiber of Figure 17a without the cell body, but with the stimulus polarity reversed. These results indicate that the presence of the cell body significantly alters the distribution of sites of excitation along the fiber. The effect is clearly dependent on stimulus polarity and probably on the magnitude and shape of the extracellular potential profile. These findings may help explain the bimodal latency distributions of single units to biphasic pulsatile stimuli [12, 14, 15] and of compound action potentials to monophasic stimuli [39]. Both of these phenomena are under active investigation using the integrated field-neuron model. In any case, realistic models of neuronal responsiveness to electrical stimulation must account for these mechanisms.

An additional phenomenon to be incorporated into these models is the stochastic behavior of the neuron. Verveen [41] has shown that neuronal responsiveness to electrical stimulation fluctuates over time in a manner that is consistent with the presence of noise sources at the nodal membrane.

Threshold fluctuations are observed routinely in recordings of electrically stimulated VIII nerve fibers [14]. We have shown that a model based on simple anatomical measurements of nodal membrane area can predict the shape of these fibers' probability-of-firing input-output functions [42]. When combined with the anatomical variability that exists among fibers [19], we expect that stochastic neuronal behavior will significantly effect the responsiveness of the general population of fibers comprising an ensemble. Such a stochastic model of neuronal responsiveness to electrical stimulation is proving useful in predicting psychometric, intensity discrimination and dynamic range functions.

G. Summary

Although simple in principle, the mechanisms involved in electrical stimulation of the cochlea are very complex in practice. We have presented an integrated field-neuron model that describes first the electrical field patterns for a variety of electrode systems and then the responsiveness of neurons lying in those electrical fields. The electrical fields are strongly dependent on the configuration and placement of the electrode array, as is the neuronal responsiveness on the location, anatomy, and physiology of the fiber itself. In addition, to fully describe the consequences of electrical stimulation within the cochlea, the aggregate response of an ensemble of simultaneously stimulated fibers must be considered as well.

When considered en mass, the electrically stimulated cochlea appears as a highly non-linear, uncontrollable interface that limits the ultimate performance goals of cochlear prostheses. However, electrical stimulation of the cochlea also can be considered as an ordered set of biophysically-based mechanisms, each contributing to the overall response pattern in a systematic manner. Knowledge of these mechanisms will allow us to identify the fundamental limitations of the peripheral electrical interface and will provide many opportunities for optimization of electrode systems and stimulation protocols. Such research will ultimately lead both to improved cochlear prostheses and greater insight into basic hearing mechanisms.

H. Acknowledgments

This work was supported by NIH contracts N01-NS-3-2356 and N01-NS-5-2396 from the Neural Prosthesis Program of NINCDS and a Professional Development Award from Research Triangle Institute to CCF. The authors are indebted to F. Terry Hambrecht for continued encouragement and support and to Dewey T. Lawson for editorial review.

I. References

[1] von Békésy G (1951) The Course Pattern of the Electrical Resistance in the Cochlea of the Guinea Pig (Electro-Anatomy of the Cochlea). Reprinted in von Békésy G (1960) Experiments in Hearing. McGraw-Hill, New York, p. 684-703

[2] Black RC and Clark GM (1980) Differential electrical excitation of the auditory nerve. J. Acoust. Soc. Am. 67: 868-874

[3] Cannon, MW (1976) Electrical Impedances, Current Pathways and Voltage Sources in the Guinea Pig Cochlea. Special Report ISR-S-14, Institute for Sensory Research, Syracuse University, Syracuse, New York

[4] Coburn B (1980) Electrical stimulation of the spinal cord: Two-dimensional finite element analysis with particular reference to epidural electrodes. Med. Biol. Eng. Comp. 18: 573-584

[5] Colombo J and Parkins CW (1987) A model of electrical excitation of the mammalian auditory-nerve neuron. Hearing Research 31: 287-312

[6] Finley CC, Wilson BS (1985) An integrated field-neuron model of electrical stimulation by intracochlear scala tympani electrodes. Abstr. Eighth Midwinter Res. Mtg. of the Association for Research in Otolaryngology , Clearwater Beach, FL, pp. 105-106

[7] Finley CC, Wilson, BS, White MW (1987) A finite-element model of bipolar field patterns in the electrically stimulated cochlea - a two-dimensional approximation. Proceedings of the Ninth Annual Conference of the IEEE Engineering in Medicine and Biology Society 4: 1901-1903

[8] Frankenheuser B and Huxley AF (1964) The action potential in the myelinated nerve fiber of Xenopus laevis as computed on the basis of voltage clamp data. J. Physiol. (London) 171: 302-315

[9] Grizon G (1987) Investigation of current flow in the inner ear during electrical stimulation of intracochlear electrodes. MS Thesis in Electrical Engineering and Computer Science, Mass. Institute of Technology

[10] Hinojosa R and Marion M (1983) Histopathology of profound sensorineural deafness. Ann. N.Y. Acad. Sci. 405: 459-484

[11] van den Honert C and Stypulkowski PH (1987) Single fiber mapping of spatial excitation patterns in the electrically stimulated auditory nerve. Hearing Research 29: 195-206

[12] van den Honert C and Stypulkowski PH (1987) Temporal response patterns of single auditory nerve fibers elicited by periodic electrical stimuli. Hearing Research 29: 207-222

[13] Honrubia V, Strelioff D, and Sitko S (1974) Electroanatomy of the Cochlea: Its Role in Cochlear Potential Measurements. Proceedings of the International Congress in Electrocochleography. Bronx, New York

[14] Javel E, Tong YC, Shepherd RK and Clark GM (1987) Responses of cat auditory nerve fibers to biphasic electrical current pulses. Ann. Otol. Rhinol. Laryngol. 96, Suppl 128: 26-30

[15] Javel E (1989) Acoustic and electrical encoding of temporal information. In Miller JM and Spelman FA (eds.), Models of the Electrically Stimulated Cochlea, Springer-Verlag, this volume

[16] Johnstone BM, Johnstone JR, and Pugsley ID (1966) Membrane Resistance in Endolymphatic Walls of the First Turn of the Guinea-Pig Cochlea. J. Acoust. Soc. Am. 40: 1398-1404

[17] Laurence M (1980) Factors in the continuing development of auditory prostheses. In Controversies in Otolaryngology, JB Snow (ed.), Philadelphia, PA: WB Saunders pp. 433-442

[18] Leake-Jones PA and Rebscher SJ (1983) Cochlear pathology with chronically implanted scala tympani electrodes. Ann. N.Y. Acad. Sci. 405: 203-223

[19] Liberman MC and Oliver ME (1984) Morphometry of intracellularly labeled neurons of the auditory nerve: correlations with functional properties. J. comp. Neurol. 223: 163-176

[20] Loeb GE, Byers CL, Rebscher SJ, Casey DE, Fong MM, Schindler RA, Gray RF, Merzenich MM (1983) Design and fabrication of an experimental cochlear prosthesis. Med. & Biol. Eng. & Compt. 21: 241-254

[21] McNeal DR (1976) Analysis of a model for excitation of myelinated nerve. IEEE BME 23(4): 329-337.

[22] Merzenich MM and White MW (1977) Cochlear implant. The interface problem. In Functional Electrical Stimulation: Applications in Neural Prostheses, Hambrecht FT and Reswick JB (eds.), volume 3 of Biomedical Engineering and Instrumentation Series, Marcel Dekker, New York, pp. 321-340

[23] Miller CE, Henriquez CS (1988) Three-dimensional finite element solution for biopotentials: Erythrocyte in an applied field. IEEE BME 35(9): 712-718

[24] Misrahy GA, Hildreth KM, Shinabarger EW, and Gannon WJ (1958) Electrical Properties of the Wall of the Endolymphatic Space of the Cochlea (Guinea Pig). Am. J. Physiol. 194: 396-402

[25] Patrick JF, Crosby PA, Hirshorn MS, Kuzma JA, Money DK, Ridler J, Seligman PM (1985) Australian multi-channel implantable hearing prosthesis. In Cochlear Implants, Schindler RA and Merzenich MM (eds.), Raven Press, New York, pp. 93-100

[26] Pernkopf E (1960) Topographische Anatomie des Menschen IV. Band: Topograhische und stratigraphische Anatomie des Kopfes. Zweite Halfte, Urban and Schwarzenberg, Berlin, p 599 (Note: 3rd English edition published in 1989 by Urban and Schwarzenberg, Balitmore-Munich)

[27] Ranck JB (1975) Which elements are excited in electrical stimulation of mammalian central nervous system: a review. Brain Res 98: 417-440

[28] Rattay F (1986) Analysis of models for external stimulation of axons. IEEE BME 33(10): 974-977

[29] Rattay F (1987) Ways to approximate current-distance relations for electrically stimulated fibers. J. Theor. Biol. 125: 339-349

[30] Reilly JP, Freeman VT and Larkin WD (1985) Sensory effects of transient electrical stimulation - evaluation with a neuroelectric model. IEEE BME 32(12): 1001-1011

[31] Reilly JP and Bauer RH (1987) Application of a neuroelectric model to electrocutaneous sensory sensitivity: Parameter variation study. IEEE BME 34(9): 752-754

[32] Rubinstein JT, Soma M, Spelman FA (1985) Mixed boundary value problem in the implanted cochlea: An analytical model of a cylindrical banded electrode array. Proceedings of the Seventh Annual Conference of the IEEE Engineering in Medicine and Biology Society, pp. 1120-1123

[33] Shepherd RK, Clary GM, Pyman BC, Webb RL (1985) The banded intracochlear electrode array: an evaluation of insertion trauma. Ann. Otol. Rhinol. Laryngol. 94: 55-59

[34] Sitko S (1976) Electrical Network Properties of the Guinea Pig Cochlea. Doctoral Dissertation, University of California, San Diego, California

[35] Soma M, Spelman FA, Rubinstein JT (1984) Fields produced by the cochlear prosthesis: The ear as a multilayered medium. Proceedings of the IEEE Conference on Frontiers of Engineering & Computing in Health Care, pp. 401-405

[36] Spelman FA, Clopton BM, Pfingst BE (1982) Tissue impedance and current flow in the implanted ear. Implications for the cochlear prosthesis. Ann. Oto. Rhinol. and Laryngol. 91: Suppl 98, 3-

[37] Spelman FA, Clopton BM (1987) Measurement of the specific impedance of bony tissues in the guinea pig cochlea. Abst. #41 of 10th Midwinter Res. Mtg. of the Association for Research in Otolaryngology

[38] Strelioff D (1973) A computer simulation of the generation and distribution of cochlear potentials. J. Acoust. Soc. Am. 54: 620-629

[39] Stypulkowski PH and van den Honert C (1984) Physiological properties of the electrically stimulated auditory nerve. I. Compound action potential recordings. Hearing Research 14: 205-223

[40] Sweeney JD, Mortimer JJ and Durand D (1987) Modeling of mammalian myelinated nerve for functional neuromuscular stimulation. Proceedings of the Ninth Annual Conference of the IEEE Engineering in Medicine and Biology Society, Boston, MA, p. 1577

[41] Verveen AA and Derksen HE (1968) Fluctuation phenomena in nerve membrane. Proc. of the IEEE 56: 906-916

[42] White MW, Finley CC, Wilson BS (1987) Electrical stimulation model of the auditory nerve: Stochastic response characteristics. Proceedings of the Ninth Annual Conference of the IEEE Engineering in Medicine and Biology Society, Boston, MA, pp. 1906-1907

[43] Wilson BS, Finley CC (1984) Speech processors for auditory prostheses. 2nd-4th Qtr. Progress Reports, Contract No. N01-NS-3-2356, NINCDS, NIH

III. Plans for the Next Quarter

Our plans for the next quarter include the following:

1. Conduct studies with several patients implanted with the Nucleus cochlear prosthesis, with emphasis on comparison of the interleaved pulses (IP) processor and the feature-extraction processor used in the Nucleus device (these studies will be done in collaboration with investigators at the University of North Carolina and are expected to begin in late February, 1989);

2. Conduct studies with one or two patients implanted with the Symbion cochlear prosthesis, with emphasis on comparison of the IP processor and the compressed-analog processor used in the Symbion device (these studies will be done in collaboration with Don Eddington and Bill Rabinowitz of the Massachusetts Eye and Ear Infirmary, and are expected to begin in mid March, 1989);

3. Analyze the data obtained in studies with patients MC1 and MC2 in the past quarter;

4. Continue work to upgrade the Cochlear Implant Laboratory at Duke, with the aim of completing (a) the software conversion for the new 80386 machine and (b) the real-time processing code for the TMS320C25 system;

5. Attend the annual meeting of the Association for Research in Otolaryngology (ARO) in St. Petersburg, FL (Feb. 5-9, 1989);

6. Present project work in an invited lecture at the University of Iowa (March 20, 1989); and

7. Continue preparation of manuscripts for publication.

Appendix 1

Summary of Reporting Activity for the Period of
September 26 through December 26, 1988
NIH Contract N01-NS-5-2396

The following major presentations were made in the present reporting period:

Wilson, B.S.: Comparison of encoding schemes. Invited paper presented at the 25th Anniversary Symposium of the Kresge Hearing Research Institute, Ann Arbor, MI, Oct. 3-5, 1988.

Finley, C.C.: 3D finite element analysis. Invited paper presented at the 25th Anniversary Symposium of the Kresge Hearing Research Institute, Ann Arbor, MI, Oct. 3-5, 1988.

Wilson, B.S.: Speech processors for auditory prostheses. Presented at the Nineteenth Neural Prosthesis Workshop, National Institutes of Health, Bethesda, MD, Oct. 26-28, 1988.

Finley, C.C.: Finite element modeling of intracochlear electrodes. Presented at the Nineteenth Neural Prosthesis Workshop, National Institutes of Health, Bethesda, MD, Oct. 26-28, 1988.

In addition, the following two papers were accepted for publication:

Wilson, B.S., Finley, C.C., and Lawson, D.T.: Representations of speech features with cochlear implants. To appear in J.M. Miller and F.A. Spelman (Eds.), Models of the Electrically Stimulated Cochlea, Springer-Verlag.

Finley, C.C., Wilson, B.S., and White, M.W.: Models of neural responsiveness to electrical stimulation. To appear in J.M. Miller and F.A. Spelman (Eds.), Models of the Electrically Stimulated Cochlea, Springer-Verlag.